

‘Exact’ solutions of the full electrokinetic model for soft spherical colloids: Electrophoretic mobility

Reghan J. Hill *

*Department of Chemical Engineering and McGill Institute for Advanced Materials,
McGill University, Montreal, Quebec, H3A2B2, CANADA*

D. A. Saville

*Department of Chemical Engineering, Princeton University, Princeton, New
Jersey, 08542, USA*

Abstract

Numerical solutions of the standard electrokinetic model provide a basis for interpreting a variety of electrokinetic phenomena involving ‘bare’ colloids. However, the model rests on the classical notion of a shear or slipping plane, whose location is unknown when surfaces are coated with permeable polymer. Consequently, an electrokinetic model for ‘soft’, ‘hairy’ or ‘fuzzy’ colloids has been developed, but until recently solutions were available only for several restricted cases, most notably for particles with thin, uniform layers, and without polarization and relaxation. Here we present numerically exact solutions of the full model for a variety of soft colloids, including PEG-coated liposomes, PEO-coated latices, human erythrocytes, and polyelectrolyte micelles. Particular attention is given to linking the thickness, density and permeability of the coatings, which are key parameters in the model, to “physical” quantities, such as the polymer molecular weight, adsorbed amount, and hydrodynamic layer thickness. This paper also identifies limits—on the ionic strength, particle size, layer thickness and permeability—beyond which earlier theories breakdown. In short, polarization and relaxation are as influential on the mobility of soft colloids as they are for ‘bare’ particles.

Key words: electrophoretic mobility, electrokinetic phenomena, soft colloids, polymer-coated colloids, sterically stabilized colloids, stealth liposomes, human erythrocytes, charged micelles

PACS:

Contents

1	Introduction	3
2	Theory	4
2.1	The electrokinetic transport equations	5
2.2	Inner (particle surface) boundary conditions	6
2.3	Outer (far-field) boundary conditions	7
2.4	Solution of the equations	7
2.5	Equilibrium state	8
2.6	Linearized perturbed state	8
2.7	Measurable quantities derived from the solution	9
2.8	Polymer layer characterization	11
3	The mobility of colloids with neutral coatings	12
3.1	Connection of the electrophoretic mobility to the hydrodynamic layer thickness	12
3.2	Thin coatings and passage to the high-ionic-strength limit	15
3.3	Polarization and relaxation, and the influence of particle size	16
3.4	Interpreting experiments	17
3.5	Terminally anchored PEG on lipid bilayer membranes (stealth liposomes)	21
3.6	PEO adsorbed on polystyrene latices	22
4	The mobility of colloids with charged coatings	27
4.1	Thin polyelectrolyte coatings	27
4.2	Glycocalyx on human erythrocytes	29
4.3	Poly(styrene sulfonate) micelles	30
5	Summary	34

* Corresponding author

Email address: `reghan.hill@mcgill.ca` (Reghan J. Hill).

1 Introduction

Polymer deposited on the surface of ‘bare’ colloidal particles can be used to regulate the stability and rheology of dispersions; the influence of *thin* polymer coatings on the drag coefficient and intrinsic viscosity, for example, are available from exact solutions of the Stokes equations (1). In addition, adjusting the electrostatic, steric, and dispersive contributions to the inter-particle potential affords control over the kinetics and thermodynamics of self-assembly processes. In turn, these bear directly on the microstructure of materials with novel properties. Nevertheless, the polymer coating density, thickness and charge affect electrokinetic transport processes near the supporting surface, making it difficult to discern competing influences that affect light scattering and electrophoresis measurements, for example. Clearly, the application of polymer coatings for tailoring the properties of dispersions will benefit from a reliable electrokinetic theory.

The purpose of this paper is to describe applications of a recently developed model for predicting the influence of polymer coatings on a variety of electrokinetic particle characterization measurements. The focus of this paper is on the electrophoretic mobility, but it should be kept in mind that the model permits solutions under dynamic conditions, as encountered in dielectric relaxation spectroscopy and electro-sonic-amplitude devices.

While the electrokinetics of bare particles are (relatively) well understood, the situation for colloids coated with a permeable polymer is less established. With bare particles, ion transport and hydrodynamics follow classical models, where, for example, hydrodynamic shear begins at the particle surface (shear surface). Efforts to model transport processes inside a thin porous layer have adopted a variety of approaches (2; 3). More realistic (and physically appealing) models treat polymer layers as continuous porous media with a permeability that reflects the density and hydrodynamic size of the polymer segments.

Charged layers, which are important because of their biological context, present a challenging set of problems. A variety of approximations have been used to construct tractable models, but, until recently, none had the generality of O’Brien and White’s numerical solution of the standard model for bare particles (4). For example, Brooks and coworkers developed models for human erythrocytes (red blood cells), with ‘flat’, uniformly charged layers to mimic the extracellular glycocalyx layer (5; 6); Hermans and Fujita considered porous charged spheres (7; 8); and, more recently, Ohshima and coworkers generalized these models, presenting approximate solutions (for the electrophoretic mobility) that neglect, in particular, polarization and relaxation (9; 10).

Without exact solutions, the accuracy of approximations is unknown, so empir-

ical parameters derived from experiments using approximate theories should be accepted with caution. Saville demonstrated that even ‘large’ particles with thin polymer and diffuse double layers are susceptible to polarization and relaxation (11). Inferences drawn from his semi-analytical theory have been borne by numerically exact solutions of the full model (12), and recent attention has turned to details of the polymer segment density distribution (13).

This paper reviews the full electrokinetic model for colloids with soft neutral and charged layers. We draw upon numerically exact solutions of the governing equations, as provided by Hill, Saville and Russel’s model (12). Their methodology removes all restrictions imposed by earlier approximate theories, permitting studies that examine the influence of particle size and polymer-layer structure in considerable detail. Accordingly, this paper establishes the parameter spaces of earlier approximate theories as limiting cases of the full model.

We begin with a presentation of the full electrokinetic model (§ 2), linking the solution of the equations to the mobility and effective layer thickness (§ 2.7), and briefly discussing key parameters that characterize polymer layers (§ 2.8). Next, the results are presented, beginning with particles that have *neutral* polymer coatings (§ 3). First, we highlight the significant role of the hydrodynamic layer thickness, distinguishing it from the actual thickness (§3.2). Detailed comparisons are made with Ohshima’s theories for thin coatings at high ionic strength, and, in particular, establishing the significance of polarization and relaxation (§ 3.3). Next, a methodology for interpreting experimental data is presented (§ 3.4), and the full model is then applied to interpret the mobilities of stealth liposomes (§ 3.5) and PEO-coated latices (§ 3.6). Turning to particles with *charged* layers (§ 4), we compare the full model with approximate theories for thin layers (§ 4.1). ‘Exact’ calculations are presented for human erythrocytes (§ 4.2) and ‘small’, highly charged polyelectrolyte micelles (§ 4.3). We conclude with summary (§ 5).

2 Theory

The electrokinetic model and the computational methodology adopted in this work have been described in detail by Hill, Saville and Russel (12). The model augments the standard electrokinetic model for bare colloids (4) with arbitrary (radial) distributions of Stokes resistance centers and charge. Electroosmotic flow within the polymer layer is hindered by hydrodynamic drag on the segments. In this work, electromigration and molecular diffusion are unaltered, which is reasonable when (*i*) the hydrodynamic volume fraction of the ions is low and (*ii*) the ions are small compared to the polymer interstices, *i.e.*, the polymer volume fraction is low. In principle, however, the methodology per-

mits the introduction of spatially dependent ion mobilities, solvent viscosity and dielectric constant.

2.1 The electrokinetic transport equations

The transport equations and boundary conditions are presented here in dimensional form. As usual, they comprise the non-linear Poisson-Boltzmann equation

$$\epsilon_o \epsilon_s \nabla^2 \psi = - \sum_{j=1}^N (n_j - n_j^f) z_j e, \quad (1)$$

where ϵ_o and ϵ_s are the permittivity of a vacuum and dielectric constant of the electrolyte (solvent); n_j and n_j^f are the concentrations of the j th mobile and fixed charges, with z_j the valences¹; e is the elementary charge and ψ the electrostatic potential.

Transport of the mobile ions is governed by

$$6\pi\eta a_j (\mathbf{u} - \mathbf{v}_j) - z_j e \nabla \psi - kT \nabla \ln n_j = 0 \quad (j = 1, \dots, N), \quad (2)$$

where a_j are Stokes radii, obtained from limiting conductances or diffusivities; η is the electrolyte viscosity, and \mathbf{u} and \mathbf{v}_j are the fluid and ion velocities; kT is the thermal energy.

Ion conservation demands

$$\partial n_j / \partial t = -\nabla \cdot (n_j \mathbf{v}_j) \quad (j = 1, \dots, N), \quad (3)$$

where t denotes time, with the ion fluxes $\mathbf{j}_j = n_j \mathbf{v}_j$ obtained from Eqn. (2).

Similarly, momentum and mass conservation require

$$\rho_s \partial \mathbf{u} / \partial t = \eta \nabla^2 \mathbf{u} - \nabla p + \eta / \ell^2 (\mathbf{V} - \mathbf{u}) - \sum_{j=1}^N n_j z_j e \nabla \psi \quad (4)$$

and

$$\nabla \cdot \mathbf{u} = 0, \quad (5)$$

where ρ_s and \mathbf{u} are the electrolyte (solvent) density and velocity, and p is the pressure. Note that $\eta / \ell^2 (\mathbf{V} - \mathbf{u})$ represents the hydrodynamic drag force exerted by the polymer on the interstitial fluid, with ℓ^2 the (radially varying) permeability of the polymer, and \mathbf{V} is the particle velocity. Clearly, the polymer and particle are assumed to move as a rigid composite, and the particle Reynolds number $\text{Re} = Va\rho_s/\eta$ is assumed small.

¹ The valence of the fixed charge is set opposite to that of its respective (mobile) counterion in Eqn. (1)

As usual, the double-layer thickness

$$\kappa^{-1} = [kT\epsilon_s\epsilon_o/(2Ie^2)]^{1/2} \quad (6)$$

emerges from Eqns. (1) and (2) where

$$I = (1/2) \sum_{j=1}^N z_j^2 n_j^\infty \quad (7)$$

is the bulk ionic strength, with n_j^∞ the bulk ion concentrations. Note that ion diffusion coefficients are

$$D_j = kT/(6\pi\eta a_j), \quad (8)$$

and the permeability (square of Brinkman screening length) may be expressed as

$$\ell^2 = 1/(n6\pi a_s F_s) = 2a_s^2/(9\phi_s F_s), \quad (9)$$

where $n(r)$ is the concentration of Stokes resistance centers (segments), with a_s and $F_s(\phi_s)$ the Stokes radius and drag coefficient of the segments. For the rigid, ‘random’ configurations of spherical segments assumed in this work, the segment drag coefficient varies with the hydrodynamic volume fraction $\phi_s = n(4/3)\pi a_s^3$ according to (14)

$$F_s = \frac{1 + 3(\phi_s/2)^{1/2} + (135/64)\phi_s \ln \phi_s + 16.456\phi_s}{1 + 0.681\phi_s - 8.48\phi_s^2 + 8.16\phi_s^3} \quad (\phi_s < 0.4). \quad (10)$$

The numerator in Eqn. (10) derives from theory for low to moderate volume fractions (15), with the denominator providing a smooth transition through data from multipole simulations ($\phi_s < 0.4$) to the well-known Carman correlation ($0.4 < \phi_s < 0.64$). Note that other drag-coefficient correlations exist for *porous media* with ordered and other random microstructures (see 16; 17, for fibrous microstructures). At present, however, such details are of secondary importance to the distribution of segments $n(r)$ and their size a_s . The segment and fixed-charge density distributions are discussed in section 2.8, and throughout sections 3 and 4.

2.2 Inner (particle surface) boundary conditions

The model permits either the equilibrium surface potential ζ or surface charge density σ_c to be specified. Because the surface ($r = a$) is assumed impermeable, the surface charge is constant under the influence of an external electric field or particle motion. This is achieved with no-flux boundary conditions for each (mobile) ion species. As usual, the no-slip boundary condition applies to the electrolyte. It follows that (inner) boundary conditions are either

$$\psi = \zeta \text{ at } r = a \quad (11)$$

or

$$\epsilon_s \epsilon_o \nabla \psi|_{out} \cdot \hat{\mathbf{n}} - \epsilon_p \epsilon_o \nabla \psi|_{in} \cdot \hat{\mathbf{n}} = -\sigma_c \text{ at } r = a, \quad (12)$$

with

$$n_j \mathbf{v}_j \cdot \hat{\mathbf{n}} = 0 \text{ at } r = a \quad (j = 1, \dots, N) \quad (13)$$

and

$$\mathbf{u} = \mathbf{V} \text{ at } r = a. \quad (14)$$

Note that $\hat{\mathbf{n}} = \mathbf{e}_r$ is an outward unit normal and $\mathbf{r} = r\mathbf{e}_r$ is the (radial) distance from the center of the particle. The dielectric constant of the bare particle ϵ_p does not affect the electrophoretic mobility to linear order in the applied electric field (4), but it is relevant under dynamic (high-frequency) forcing, such as in dielectric spectroscopy.

2.3 Outer (far-field) boundary conditions

Particle interactions are neglected, so an otherwise stationary, infinite domain leads to far-field boundary conditions

$$\psi \rightarrow -\mathbf{E} \cdot \mathbf{r} \text{ as } r \rightarrow \infty, \quad (15)$$

$$n_j \rightarrow n_j^\infty \text{ as } r \rightarrow \infty \quad (j = 1, \dots, N), \quad (16)$$

and

$$\mathbf{u} \rightarrow 0 \text{ as } r \rightarrow \infty, \quad (17)$$

where \mathbf{E} is a uniform applied electric field.

2.4 Solution of the equations

Coupling the transport equations and boundary conditions to the particle equation of motion specifies the electrokinetic model². As usual, the solution requires non-linear perturbations to the equilibrium state to be neglected. Perturbations (proportional to the applied electric field) are introduced via

$$\psi = \psi^0 - \mathbf{E} \cdot \mathbf{r} + \psi', \quad (18)$$

$$n_j = n_j^0 + n'_j \quad (j = 1, \dots, N), \quad (19)$$

and

$$p = p^0 + p', \quad (20)$$

² A computer package (MPEK) implementing Hill, Saville and Russel's methodology is currently available from the corresponding author.

where the first terms on the right-hand sides denote the equilibrium values, and the primed quantities denote the perturbations.

2.5 Equilibrium state

When $\mathbf{E} = \mathbf{V} = 0$, equilibrium is specified according to

$$\epsilon_o \epsilon_s \nabla^2 \psi^0 = - \sum_{j=1}^N (n_j^0 - n_j^f) z_j e, \quad (21)$$

$$0 = -\nabla \cdot [-D_j \nabla n_j^0 - z_j e D_j / (kT) n_j^0 \nabla \psi^0] \quad (j = 1, \dots, N), \quad (22)$$

and

$$0 = -\nabla p^0 - \sum_{j=1}^N n_j^0 z_j e \nabla \psi^0, \quad (23)$$

with either

$$\psi^0 = \zeta \quad (24)$$

or

$$\epsilon_s \epsilon_o \nabla \psi^0|_{out} \cdot \mathbf{e}_r - \epsilon_p \epsilon_o \nabla \psi^0|_{in} \cdot \mathbf{e}_r = -\sigma_c \text{ at } r = a, \quad (25)$$

$$[-D_j \nabla n_j^0 - z_j e D_j / (kT) n_j^0 \nabla \psi^0] \cdot \mathbf{e}_r = 0 \text{ at } r = a \quad (j = 1, \dots, N), \quad (26)$$

and

$$\psi^0 \rightarrow 0 \text{ as } r \rightarrow \infty, \quad (27)$$

$$n_j^0 \rightarrow n_j^\infty \text{ as } r \rightarrow \infty \quad (j = 1, \dots, N). \quad (28)$$

2.6 Linearized perturbed state

Under periodic forcing

$$\mathbf{E} = E \exp(-i\omega t) \mathbf{e}_z, \quad (29)$$

with frequency $\omega/(2\pi)$, axisymmetric perturbations take the forms

$$\psi' = \hat{\psi}(r) \mathbf{E} \cdot \mathbf{e}_r, \quad (30)$$

$$n'_j = \hat{n}_j(r) \mathbf{E} \cdot \mathbf{e}_r \quad (j = 1, \dots, N) \quad (31)$$

and

$$\mathbf{u} = -2(h_r/r)(\mathbf{E} \cdot \mathbf{e}_r) \mathbf{e}_r - (h_{rr} + h_r/r)(\mathbf{E} \cdot \mathbf{e}_\theta) \mathbf{e}_\theta, \quad (32)$$

where

$$\mathbf{u} = \nabla \times \nabla \times h(r)\mathbf{E}. \quad (33)$$

The perturbations satisfy

$$\epsilon_o \epsilon_s \nabla^2 \psi' = - \sum_{j=1}^N n'_j z_j e, \quad (34)$$

$$\partial n'_j / \partial t = -\nabla \cdot \mathbf{j}'_j \quad (j = 1, \dots, N), \quad (35)$$

where

$$\mathbf{j}'_j = -D_j \nabla n'_j - z_j e D_j / (kT) n'_j \nabla \psi^0 - z_j e D_j / (kT) n_j^0 (\nabla \psi' - \mathbf{E}) + n_j^0 \mathbf{u}, \quad (36)$$

$$\rho_s \partial \mathbf{u} / \partial t = \eta \nabla^2 \mathbf{u} - \nabla p' - \eta / \ell^2 (\mathbf{u} - \mathbf{V}) - \sum_{j=1}^N n_j^0 z_j e (\nabla \psi' - \mathbf{E}) - \sum_{j=1}^N n'_j z_j e \nabla \psi^0 \quad (37)$$

and

$$\nabla \cdot \mathbf{u} = 0, \quad (38)$$

with

$$\epsilon_s \epsilon_o (\nabla \psi' - \mathbf{E})|_{out} \cdot \mathbf{e}_r - \epsilon_p \epsilon_o (\nabla \psi' - \mathbf{E})|_{in} \cdot \mathbf{e}_r = 0 \text{ at } r = a, \quad (39)$$

$$\mathbf{j}'_j \cdot \mathbf{e}_r = 0 \text{ at } r = a \quad (j = 1, \dots, N), \quad (40)$$

$$\mathbf{u} = \mathbf{V} \text{ at } r = a, \quad (41)$$

and

$$\psi' \rightarrow 0 \text{ as } r \rightarrow \infty, \quad (42)$$

$$n'_j \rightarrow 0 \text{ as } r \rightarrow \infty \quad (j = 1, \dots, N), \quad (43)$$

$$\mathbf{u} \rightarrow 0 \text{ as } r \rightarrow \infty. \quad (44)$$

2.7 Measurable quantities derived from the solution

The linearized equations and boundary conditions, which are characterized by multiple and widely varying length scales, are solved using the methodology described in detail by Hill, Saville and Russel (see 12). In practice, the

equations are solved with the particle fixed at $\mathbf{r} = \mathbf{0}$, with (i) a prescribed far-field velocity $-\mathbf{V}$ and $\mathbf{E} = \mathbf{0}$ —the so-called (U) problem, or (ii) a prescribed electric field \mathbf{E} and stationary far-field—the so-called (E) problem. These solutions are superposed to satisfy the particle equation of motion (see 4; 12), which leads to the *electrophoretic* mobility,

$$V/E = C^E/C^U, \quad (45)$$

where

$$C^X = \lim_{r \rightarrow \infty} h_r^X. \quad (46)$$

Under oscillatory conditions, the *dynamic mobility* is

$$V/E = C^E/[C^U - (\kappa a)^3(\rho_p - \rho_s)/(3\rho_s)], \quad (47)$$

where

$$C^X = \lim_{r \rightarrow \infty} h_r^X r^2 \quad (48)$$

and ρ_p is the density of the bare particle. Note that the superscripts $X \in \{U, E\}$ denote the (U) and (E) problems, where C^X are “asymptotic coefficients” that characterize the far-field decay of $h(r)$ in Eqn. (33).

Following standard convention, the scaled *electrophoretic mobility* is defined as

$$M = (V/E)3\eta e/(2\epsilon_s \epsilon_o kT), \quad (49)$$

so the well-known Hückel and Smoluchowski mobilities are $M = \zeta$ and $M = (3/2)\zeta$, where ζ is scaled with kT/e .

The *drag coefficient*

$$F = f/(6\pi\eta aV) \quad (50)$$

is the force f required to translate the particle with velocity V in the absence of an applied electric field, scaled with the Stokes drag force on the bare uncharged sphere. Frictional drag on the polymer coating and electro-viscous effects arising from charge increase the effective particle size. This motivates our definition of an *effective coating thickness*

$$L_e = a(F - 1), \quad (51)$$

which, in the absence of electro-viscous stresses, is termed the *hydrodynamic coating thickness*

$$L_h = L_e \text{ when } \sigma_c = n_j^f = 0. \quad (52)$$

In practice, the hydrodynamic coating thickness is realized when the surface potential is low, which is often the case at high ionic strength.

2.8 Polymer layer characterization

The length and molecular weight of a polymer segment, l and M_s , and the number of segments per chain N are defined so the chain contour length and molecular weight are $l_c = Nl$ and $W = NM_s$. If the segments are monomer units, then l and N are denoted l_m and N_m , so $l_c = N_m l_m$ and $W = N_m M_m$. Similarly, if the segments are defined as statistical or Kuhn segments, then the mean-squared end-to-end distance of a free chain in a theta solvent is $R = lN^{1/2} = l[(M/M_m)(l_m/l)]^{1/2}$, giving

$$l = R^2 M_m / (M l_m). \quad (53)$$

This is useful because R can be expressed in terms of the hydrodynamic radius and radius of gyration of ‘free’ polymer chains, and l_m is usually known from X-ray crystallography or knowledge of bond lengths and monomer architecture.

The mass of polymer per unit area of substrate is

$$W \sigma_p = N M_s \sigma_p = N_m M_m \sigma_p, \quad (54)$$

where σ_p is the number of chains per unit of surface area. The number of segments per unit volume n is often scaled to give a volume fraction $\phi = n l^3$. The ‘actual’ volumes of a solvent molecule and a polymer segment are v_1 and v_2 , so the physical volume fraction of polymer is $n v_2$. Similarly, the hydrodynamic volume fraction of polymer segments is $\phi_s = n(4/3)\pi a_s^3$, where a_s is the hydrodynamic (Stokes) radius of a segment.

The grafting density is often scaled to give $\sigma_p l^2$, but a better qualitative ‘measure’ of the grafting density is, perhaps, $\sigma_p R^2 = \sigma_p N l^2 = \sigma_p (W/M_m) l_m l$. When $\sigma_p N l^2 \sim 1$, the layer is considered semi-dilute ($\phi \ll 1$) and, therefore, laterally homogeneous. When $\sigma_p N l^2 < 1$, however, the layer is dilute and, therefore, laterally inhomogeneous. Moreover, when $\sigma_p N l^2 > 1$, layers are homogeneous throughout and are referred to as brush-like. This ‘picture’ applies to di-block copolymers where one (shorter) block anchors the other (longer) block to the substrate. The segments of adsorbed homopolymers interact strongly with the surface, giving rise to a dense inner region with a sparse periphery. The structure of polyelectrolytes is more complicated, since the statistical segment length varies with the bulk ionic strength and the degree of counterion dissociation, the latter of which may depend on the ionic strength and pH (18).

3 The mobility of colloids with neutral coatings

3.1 Connection of the electrophoretic mobility to the hydrodynamic layer thickness

In contrast to approximate analytical solutions, numerically exact solutions of the full electrokinetic model permit arbitrary segment and charge density distributions. Here we compare the electrophoretic mobilities of particles with uniform and non-uniform (Gaussian-like) layers, each with the same adsorbed amount and the same hydrodynamic layer thickness. In turn, the hydrodynamic layer thickness emerges as a characteristic of prime importance.

Gaussian-like distributions

$$n(r) = n_1 \exp[-(r - a)^2/\delta^2] \quad (r > a), \quad (55)$$

where n_1 specifies the density at the bare surface ($r = a$) and δ characterizes the layer thickness, mimic terminally anchored polymer in a theta solvent when the molecular weight and grafting density are moderately low. Substituting Eqn. (55) into the general relationship

$$N\sigma_p a^2 = \int_a^\infty n(r)r^2 dr, \quad (56)$$

where σ_p is the chain grafting density and N is the number of segments per chain, gives

$$N\sigma_p a^2 = (n_1\delta^3/4)\{\sqrt{\pi}[2(a/\delta)^2 + 1] + 4a/\delta\}. \quad (57)$$

Similarly, for a uniform distribution with density n_0 and thickness L ,

$$N\sigma_p a^2 = (n_0/3)a^3[(1 + L/a)^3 - 1]. \quad (58)$$

Let us consider how either n_1 and δ or n_0 and L are related to the electrophoretic mobility and hydrodynamic layer thickness L_h , both of which are routinely measured. Because L_h depends on the permeability $\ell^2 = 1/(6\pi n(r)a_s)$, the Stokes radius of the segments a_s must be correctly specified; here, $a_s = 0.175 \text{ \AA}$ is a value for poly(ethylene glycol) (PEG) that provides a good ‘fit’ of theory (with a self-consistent mean-field description of the polymer density distribution) to measured electrophoretic mobilities (13). The physical characteristics of four representative coatings, each decorating the surface of an impermeable spherical colloid with surface charge density $\sigma_c \approx -0.78 \mu\text{Ccm}^{-2}$ and radius $a = 500 \text{ nm}$ are listed in table 1. Each of the four sets of parameters (cases 1–4), which specify L_h and N (columns 2 and 3), have been used to characterize Gaussian-like *and* uniform (step-like) segment density distributions.

Table 1

Parameters that characterize the layers whose segment density distributions and electrophoretic mobilities are shown in figures 1 and 2: $\sigma_p l^2 = 0.072$ with $l = 0.71$ nm; $a_s = 0.175$ Å; $a = 500$ nm; $\sigma_c = -0.780$ μCcm^{-2} .

case	L_h (nm)	N	Gaussian-like		Step-like		
			n_1 (M)	δ (nm)	n_0 (M)	L (nm)	ℓ (nm)
1	28	46.2	0.63	18.8	0.32	31.8	3.9
2	23	18.5	0.25	18.8	0.14	29.3	6.0
3	14	18.2	0.38	12.5	0.22	18.7	4.8
4	7.4	9.10	0.25	9.4	0.16	12.8	5.6

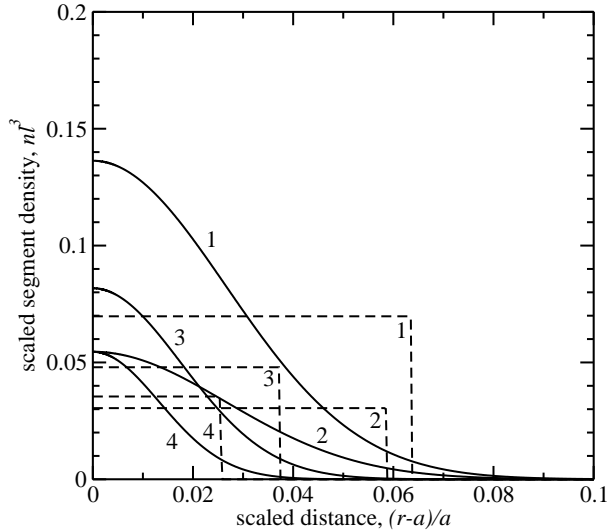


Fig. 1. The (scaled) segment density distributions $\phi(r) = n(r)l^3$ as a function of the (scaled) distance from the bare surface $(r - a)/a$ for the particles whose electrophoretic mobilities are shown in figure 2. The density and thickness of the uniform layers (*dashed* lines) have been adjusted to have (i) the same hydrodynamic layer thickness L_h and (ii) the same number of polymer segments $N\sigma_p$ as the corresponding non-uniform layer. See table 1 for the coating parameters, and figure 2 for the electrophoretic mobilities.

Note that the hydrodynamic layer thicknesses were established iteratively from solutions of problem (U) at high ionic strength. Clearly, the various molecular weights and hydrodynamic coating thicknesses lead to a variety of physical thicknesses (δ and L) and densities (n_0 and n_1). As shown in figure 1, the extent (maximum density) of each non-uniform layer is significantly greater (less) than that of its uniform counterpart.

The electrophoretic mobilities are shown in figure 2 over a range of ionic strengths. Despite large variations in density and extent, constraining each

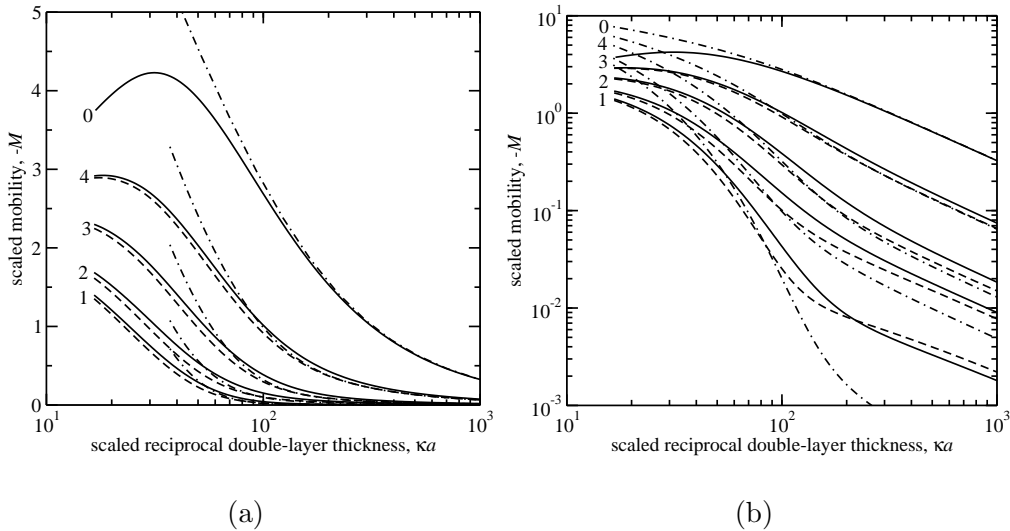


Fig. 2. The (scaled) electrophoretic mobility $M = 3\eta eV / (2\epsilon_s \epsilon_o kTE)$ as a function of the (scaled) reciprocal double-layer thickness κa (aqueous NaCl at $T = 25^\circ\text{C}$ with radius $a = 500$ nm). The surface charge density $\sigma_c \approx -0.780 \mu\text{Ccm}^{-2}$ at all ionic strengths. *Solid* lines are the full model with non-uniform segment density distributions (*solid* lines in figure 1), *dashed* lines are the full model with uniform (step-like) segment density distributions (*dashed* lines in figure 1), and *dash-dotted* lines are Ohshima’s theory (19, Eqn. (11.4.27)). See table 1 for the coating parameters (cases 1–4, with case 0 indicating the bare particle), and figure 1 for the segment density distributions.

uniform layer (*solid* lines) to have the same hydrodynamic thickness as its respective non-uniform layer (*dashed* lines) leads to similar mobilities. This is to be expected at low ionic strength, but the close correspondence at high ionic strength is surprising. When the diffuse double layer resides mostly within the layers (at high ionic strength), the mobility is expected to be more sensitive to details of the distribution. However, when the densities and thicknesses are constrained by Eqn. (56), the mobility reflects—to a good approximation—the hydrodynamic layer thickness. Clearly, if the hydrodynamic layer thickness is known, the electrophoretic mobility has a remarkably close connection to the underlying surface charge over a wide range of ionic strengths.

The logarithmically scaled mobility axis (panel (b) in figure 2) facilitates a closer comparison of the numerically exact solutions with Ohshima’s well-known analytical approximation for thin uniform layers (19, Eqn. (11.4.27)) (*dash-dotted* lines). Good agreement is seen when $L/a < 0.02$ and $\kappa a > 100$, but, as expected, the approximate theory breaks down at low ionic strength. As shown below, Ohshima’s more complicated formula (19, Eqn. (11.4.24)) can be advantageous with higher electrostatic potentials. Here, however, the surface charge density is low enough for the breakdown to be attributed to the finite particle size, *i.e.*, to polarization and relaxation.

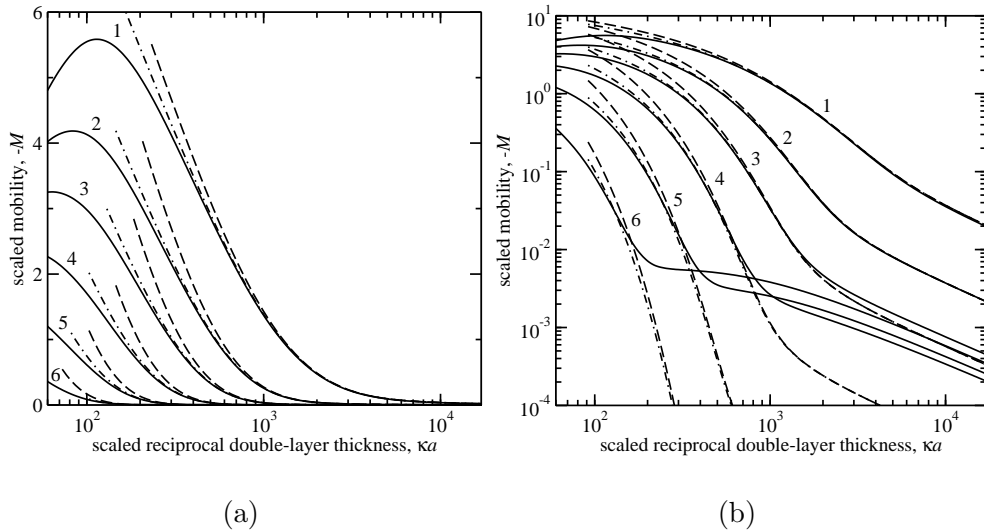


Fig. 3. The (scaled) electrophoretic mobility $M = 3\eta eV/(2\epsilon_s\epsilon_o kTE)$ as a function of the (scaled) reciprocal double-layer thickness κa (aqueous NaCl at $T = 25^\circ\text{C}$ with radius $a = 1750$ nm). The surface charge density $\sigma_c \approx -1.95 \mu\text{Ccm}^{-2}$ at all ionic strengths. *Solid* lines are the full model with uniform segment density distributions, and the *dashed* and *dash-dotted* lines are Ohshima’s theory for low (19, Eqn. (11.4.27)) and arbitrary (19, Eqn. (11.4.24)) electrostatic potentials. See table 2 for the coating parameters.

3.2 Thin coatings and passage to the high-ionic-strength limit

Surprisingly, the full model deviates from Ohshima’s flat-plate theories at high ionic strength, even with very thin layers. For example, figure 3 shows the electrophoretic mobilities of particles whose (uniform) coatings are all very thin compared to the particle radius ($a = 1750$ nm). The coating parameters and various dimensionless ratios are listed in table 2. Note that all the layers (cases 1–6) have the same grafting density and polymer molecular weight, so the increase in thickness L is accompanied by a decrease in density n_0 and, hence, an increase in permeability ℓ^2 . Nevertheless, Brinkman screening ensures that the hydrodynamic layer thickness L_h increases with L .

Despite a substantial decrease in L/a —relative to the cases presented in figure 2—there is a significant difference between the approximate and ‘exact’ results when $L/a > 0.01$. Remarkably, at high ionic strength, the mobility decreases slowly with decreasing layer thickness, whereas the flat-plate theories (*dashed* and *dash-dotted* lines) infer a monotonic decline, yielding much lower mobilities. We attribute this unexpected behavior to the finite particle size and a transition to the regime where $\kappa\ell \gg 1$ with $\ell/L \ll 1$. Note that the pressure gradient must be identically zero with a perfectly flat interface. However, when $\kappa L \gg 1$, fluid in the electrically neutral region of the polymer

Table 2

Parameters that characterize the uniform layers on particles whose electrophoretic mobilities are shown in figure 3: $\sigma_p l^2 = 0.072$ with $l = 0.71$ nm; $N = 100$; $a_s = 0.175$ Å; $a = 1750$ nm; $\sigma_c \approx -1.95 \mu\text{Ccm}^{-2}$.

case	L_h (nm)	n_0 (M)	L (nm)	ℓ (nm)	ℓ/L	L/a
1	1.10	14.0	1.69	0.591	0.35	6.3×10^{-4}
2	4.37	4.34	5.45	1.07	0.20	2.7×10^{-3}
3	8.75	2.31	10.2	1.47	0.14	0.005
4	17.5	1.20	19.6	2.04	0.10	0.01
5	35.0	0.613	37.9	2.86	0.075	0.02
6	70.0	0.307	74.0	4.04	0.055	0.04

($\kappa^{-1} < r - a < L$) must be driven by viscous stresses when $\kappa\ell > 1$. With a finite radius of curvature, radial and tangential pressure gradients then develop to move fluid through the polymer, into and out of the underlying diffuse double layer. As demonstrated by Hill, Saville and Russel (12, Fig. 6), decreasing the permeability increases the tendency of fluid to enter and exit the polymer layer radially, and this, presumably, decreases the radial and tangential pressure fluctuations.

As shown in figure 3, the breakdown of the flat-plate approximation at high ionic strength can be significant for neutral layers with moderate thickness and permeability. For example, the mobility with $L \approx 20$ nm and $\ell \approx 2$ nm (case 5) deviates from Ohshima’s theory when the ionic strength exceeds 18 mM ($\kappa a > 770$). Note that there exists an intermediate range of ionic strengths, with $\kappa\ell$ sufficiently small and κa sufficiently large, where Ohshima’s theory provides an excellent approximation. As expected, the higher surface charge here—relative to the cases presented in figure 2—demonstrates that Ohshima’s formula (19, Eqn. (11.4.24)) (*dash-dotted* lines) for arbitrary potentials can indeed provide a significantly better approximation than his simpler formula (19, Eqn. (11.4.27)) for low potentials (*dashed* lines).

3.3 Polarization and relaxation, and the influence of particle size

With polymer layers, clearly identifying the regions of the parameter space where polarization and relaxation are significant is not straightforward. The calculations presented in figures 4 and 5 systematically explore the influence of particle size ($a \approx 50$ – 3500 nm) and layer thickness. Similarly to figure 3 with $a = 1750$ nm, all the coatings have the same grafting density ($\sigma_p l^2 = 0.072$) and polymer molecular weight ($N = 100$), so the permeabilities vary with the (specified) *hydrodynamic* thickness *and* particle radius. The numerically exact

results (*solid* lines), which are compared to Ohshima’s theory for arbitrary surface potentials (19, Eqn. (11.4.24)) (*dash-dotted* lines), demonstrate how particle size influences the mobility. Because the surface charge densities are the same, varying the surface curvature is accompanied by a change in the surface potential at fixed ionic strength ($\kappa \sim \sqrt{I}$). Increasing the coating thickness decreases the mobility, mimicking the effect of decreasing the charge. As expected for bare particles, decreasing the radius increases polarization, which, in turn, decreases the mobility and shifts the maxima to smaller values of κa .

Neutral coatings attenuate polarization, however, as demonstrated by the increasing accuracy of Ohshima’s theory with increasing layer thickness when $\kappa a \approx 300$ and $a = 3500$ nm (last panel in figure 5). The close correspondence for the thickest coating ($L/a \approx 0.02$) establishes the validity of the flat-plate approximation and the negligible influence of polarization under these conditions. It follows that decreasing the layer thickness should improve the flat-plate approximation. However, the agreement clearly diminishes, and this must be attributed to polarization and relaxation. Note that decreasing the layer thickness (with $\kappa a = 300$ and $a = 3500$ nm) yields $\kappa L = 1$ when $L \approx 12$ nm. Therefore, the four thinnest layers have $\kappa L < 1$ with $\kappa a \gg 1$, this being the regime in which Saville (11) developed a semi-analytical theory to highlight the role of polarization and relaxation. Comparing the exact results with Ohshima’s theory (last panel in figure 5) confirms that polarization and relaxation can be significant when κa is large. Clearly, when most of the double layer resides beyond the polymer, *i.e.*, when $\kappa L \ll 1$, the ratio of polarization (by convection and electromigration) to relaxation (by molecular diffusion) is expected to be maximal.

3.4 *Interpreting experiments*

As shown in section 3.1, the full electrokinetic model provides satisfactory predictions of the electrophoretic mobility with uniform layers when the coating density and thickness reflect the correct adsorbed amount $\sigma_p N$ (according to Eqn. (58)) *and* the ‘correct’ hydrodynamic thickness L_h . This approach requires the Stokes radius of the polymer segments a_s to be specified. Note that, in the Brinkman model, the designation of monomer or statistical units to a polymer segment is arbitrary, as long as (i) the number of segments is unambiguously related to the molecular weight, *e.g.*, $W = NM_s = N_m M_m$ with $l_c = Nl = N_m l_m$, and (ii) the Stokes radius of the segments is appropriate.

In general, determining the hydrodynamic thickness of a layer requires a numerical solution of Brinkman’s equations or, equivalently, a solution of the (U) problem at high ionic strength. The results in table 1 for uniform layers

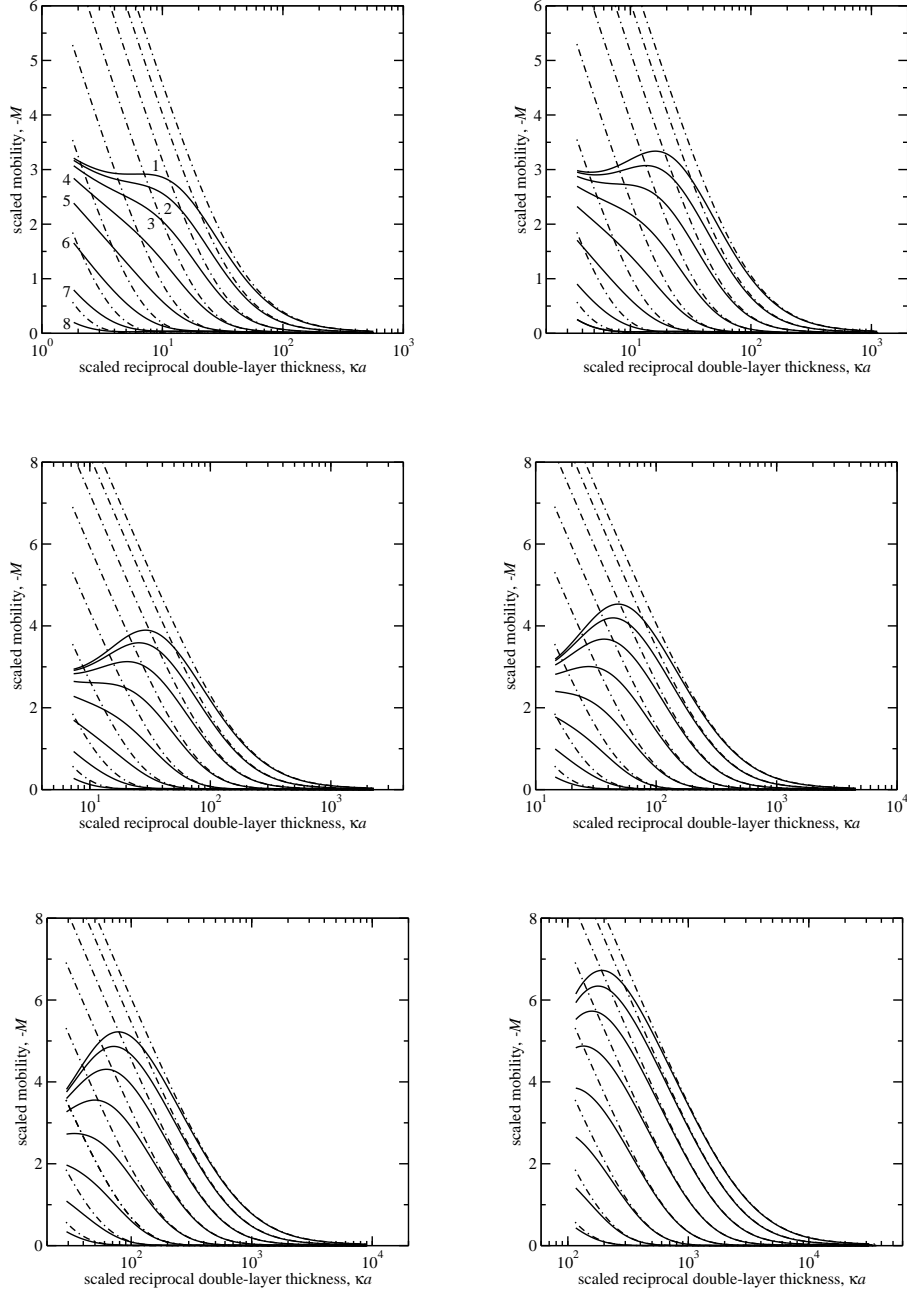


Fig. 4. The (scaled) electrophoretic mobility $M = 3\eta eV / (2\epsilon_s \epsilon_o kTE)$ as a function of the (scaled) reciprocal double-layer thickness κa (aqueous NaCl ($I = 10^{-4}$ – 10 M) at $T = 25^\circ\text{C}$ with radius $a \approx 55, 109, 219, 438, 875$ and 3500 nm (*top-left* to *bottom-right*)): $\sigma_p l^2 = 0.072$ with $l = 0.71$ nm; $N = 100$; $a_s = 0.175$ Å; $\sigma_c \approx -1.95 \mu\text{Ccm}^{-2}$. The particles have uniform neutral coatings with thicknesses L and densities n_0 specified according to Eqn. (60) with $F_s = 1$ and $L_h \approx (17.5/32)2^\nu$ nm, where $\nu = 1, 2, 3, \dots, 8$ (labeled in the first panel). *Solid* lines are the full model with uniform segment density distributions, and the *dash-dotted* lines are Ohshima's theory (19, Eqn. (11.4.24)).

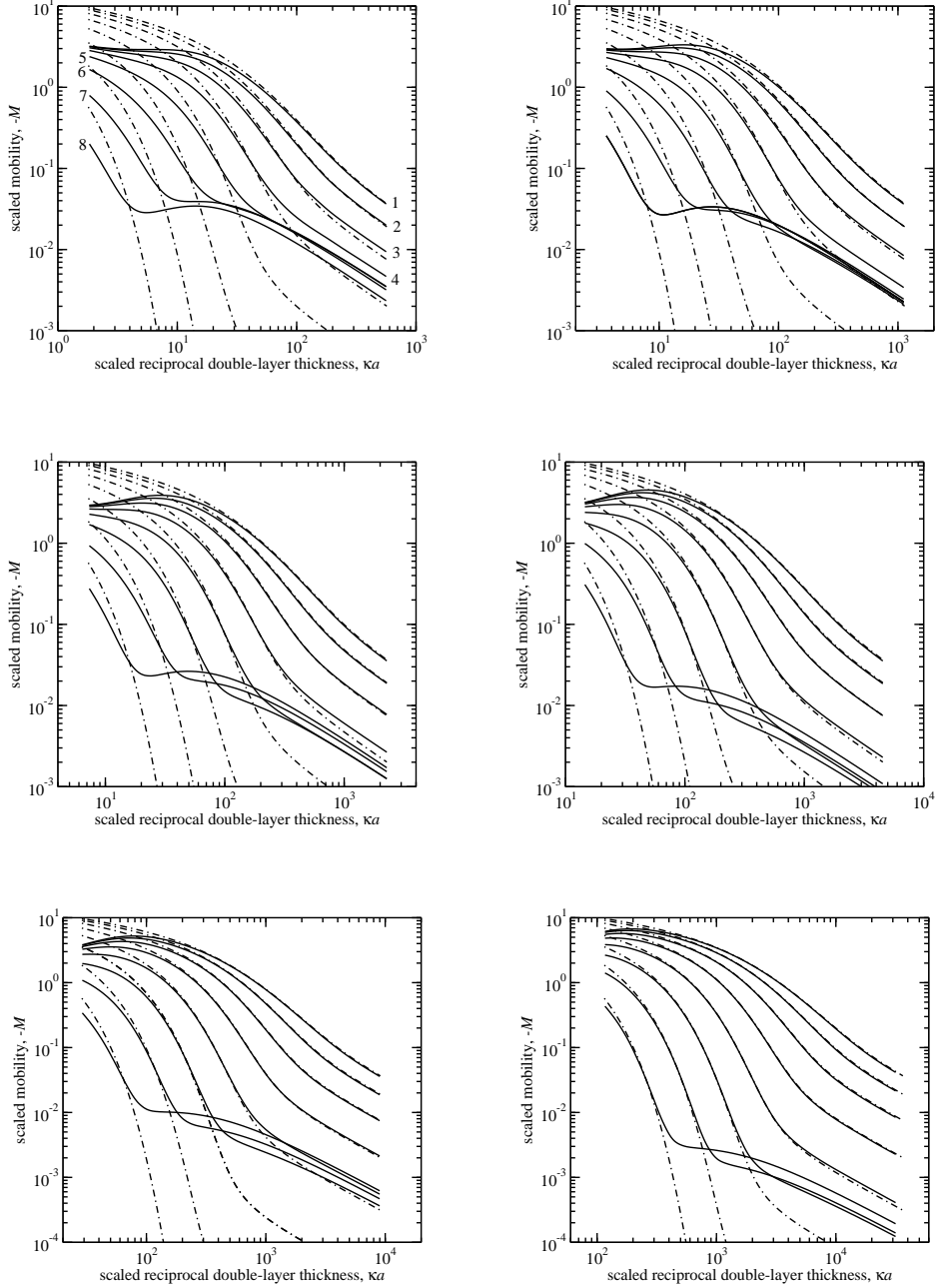


Fig. 5. As in figure 4, but with logarithmically scaled mobility axes.

demonstrate that the hydrodynamic thickness

$$L_h \approx L - \ell, \quad (59)$$

where $\ell^{-2} = 6\pi a_s F_s n_0$. It follows from Eqn. (58) that

$$(L_h - L)^2 \approx \frac{(1 + L/a)^3 - 1}{18\pi a_s F_s N \sigma_p / a}, \quad (60)$$

which is a convenient and useful formula³ relating the thickness L of a uniform layer to the physical parameters L_h , $N\sigma_p$, a_s and a . The approximation is accurate when the $O(\eta ME/\ell)$ viscous force (per unit volume) on the fluid in the layer is small relative to the $O(\eta MEL/\ell^2)$ frictional (Darcy) drag force, *i.e.*, when $\ell/L < 1$.

Equation (60) can be used to reduce the number of unknown degrees of freedom when interpreting electrokinetic experiments. Consider, for example, Cohen and Khorosheva’s experiments with poly(ethylene glycol) (PEG) terminally anchored to the surface of multilamellar liposomes with $a \approx 1750$ nm (20). Because the PEG grafting density, surface charge density, and PEG molecular weight are ‘known’, Cohen and Khorosheva devised a very simple electrokinetic model to infer a value of L and ℓ for each of the five molecular weights of PEG, *i.e.*, ten ‘fitting’ parameters. However, adopting Eqn. (60) reduces the number of such parameters to six: one value of L for each molecular weight, and one value of a_s .

Recently, Hill interpreted Cohen and Khorosheva’s experiments using a self-consistent mean-field model of the polymer segment density distribution (13). This reduced the problem to one of determining $a_s \approx 0.175$ Å alone. The remarkably small Stokes radius established for PEG statistical segments with (Kuhn) length $l = 0.71$ nm mimics the (negative) correlations that exist between micro-scale segment density and fluid velocity fluctuations, which are not explicitly accounted for in the Brinkman model (13). Physically, regions of low segment density favor high fluid velocities, thereby reducing the average drag force on an otherwise statistically homogeneous porous medium. This suggests that the Stokes radius may be a complicated function of the polymer structure and density. In relatively dense cross-linked gels, for example, density-velocity correlations may be much weaker than in brush-like layers of relatively loosely confined polymer. This would lead to a Stokes radius that is much more representative of the segment physical size.

To demonstrate the application of Eqn. (60), we adopt hydrodynamic thicknesses L_h and the segment Stokes radius $a_s \approx 0.175$ Å as established by Hill’s self-consistent mean-field description of the polymer (13), and compare the resulting mobilities with Cohen and Khorosheva’s experimental data. As shown in figure 6, the electrophoretic mobilities predicted in this manner are in good agreement with the measured values. Table 3 summarizes the parameters for each polymer molecular weight. Note that all the coatings have the same grafting density. Comparing the actual hydrodynamic thicknesses of the uniform layers (column 6) with the desired values (column 2) demonstrates that the approximation underlying Eqn. (60) is accurate when $\ell/L \ll 1$, *i.e.*, when the PEG molecular weight is greater than 1 kgmol^{-1} at this grafting

³ Eqn. (60) is easily solved iteratively, beginning with $L_h = L$.

Table 3

Parameters characterizing the polymer layers in Cohen and Khorosheva’s (CK) experiments with terminally anchored PEG on multilamellar liposomes (20). The hydrodynamic thickness of the coatings L_h and the Stokes radius of the segments $a_s \approx 0.175 \text{ \AA}$ are specified from Hill’s calculations with a self-consistent mean-field description of the polymer (13). These parameters characterize uniform layers with thickness L and permeability ℓ^2 , specified according to Eqn. (60).

W (g mol^{-1})	N	L_h ¹ (nm)	L (nm)	n_0 (M)	ℓ (nm)	L_h ² (nm)
350	4.5	0.42	5.5	0.19	5.1	1.5
1000	14	2.0	4.7	0.71	2.7	2.2
2000	28	4.3	6.5	1.0	2.2	4.3
3000	42	6.5	8.6	1.2	2.1	6.5
5000	70	11	13	1.3	2.0	11

¹ Actual or desired values from Hill’s self-consistent mean-field calculations (13).

² Actual values for uniform layers.

density. The results are also consistent with expectations that the density and, hence, permeability of polymer brushes are independent of the molecular weight at a fixed grafting density. Clearly, the Brinkman screening length decreases with increasing molecular weight, approaching $\ell \approx 2 \text{ nm}$. The layer thickness increases linearly with molecular weight, yielding $L \approx (0.21+0.22N)l$ ($l \approx 0.71 \text{ nm}$) when $W > 1 \text{ kgmol}^{-1}$. As expected, this formula is the same as Hill’s for the high-molecular-weight limit of the hydrodynamic layer thickness, $L_h \sim 0.22Nl$, at this grafting density.

3.5 Terminally anchored PEG on lipid bilayer membranes (stealth liposomes)

Cohen and Khorosheva’s experiments, introduced above, were performed with relatively large multilamellar liposomes. This permitted the particles to be observed under magnification in their electrophoresis device. However, stealth liposomes used for drug delivery have much smaller radii $a \sim 100 \text{ nm}$. With the same surface charge, polymer, and polymer grafting density, the smaller radius is expected to change the surface potential and, possibly, vary the polymer segment density distribution. Therefore, with knowledge of the Stokes radius for PEG (Kuhn) segments, obtained from Cohen and Khorosheva’s experiments with $a = 1750 \text{ nm}$, we can predict the electrophoretic mobilities of *therapeutic* stealth liposomes with $a = 100 \text{ nm}$, for example.

The polymer segment density distributions (figure 7) are from Hill’s self-consistent mean-field model (13). These calculations account for surface curvature, yielding slightly less dense layers with $a = 100 \text{ nm}$ than with $a = 1750 \text{ nm}$. The electrostatic potential is much lower, and, as expected, this

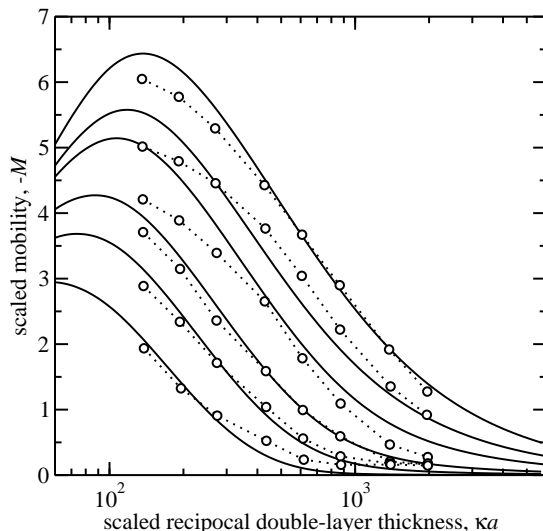


Fig. 6. The (scaled) electrophoretic mobility $M = 3\eta eV/(2\epsilon_s\epsilon_0kTE)$ of spherical liposomes with coatings of terminally anchored PEG as a function of the (scaled) reciprocal double-layer thickness κa (aqueous NaCl at $T = 25^\circ\text{C}$ with radius $a = 1750$ nm) for various numbers of statistical segments per PEG chain $N = 0, 4.5, 14, 28, 42,$ and 70 (increasing downward); the molecular weights of the PEG chains are, respectively, $W = 0, 0.35, 1, 2, 3$ and 5 kgmol^{-1} . The surface charge density $\sigma_c \approx -1.95 \mu\text{Ccm}^{-2}$ at all ionic strengths. *Circles* (with dotted lines to guide the eye) are Cohen and Khorosheva’s experimental data (20), and *solid lines* are the full model with uniform segment density distributions, whose density and thickness are chosen to yield the same hydrodynamic layer thicknesses as Hill’s self-consistent mean-field description of the layers (13). See table 3 for parameters.

changes the electrophoretic mobility, as seen by comparing the mobilities in figures 6 and 8 with $a = 1750$ and 100 nm, respectively.

3.6 PEO adsorbed on polystyrene latices

As demonstrated in section 3.4, the brush-like structure of terminally anchored PEG permits a satisfactory uniform-layer approximation when the density and thickness yield the ‘correct’ hydrodynamic coating thickness. Poly(ethylene oxide) (PEO) homopolymer, which comprises the same monomer unit as PEG, has molecular weights an order of magnitude higher. Adsorption produces much more inhomogeneous layers (see 21; 22, and the references therein), and because desorption is slow, experiments can be performed under conditions where the influence of polymer on the hydrodynamic size and electrophoretic mobility is significant, without altering the electrolyte viscosity.

Gittings and Saville (23) measured the adsorbed amounts, hydrodynamic layer

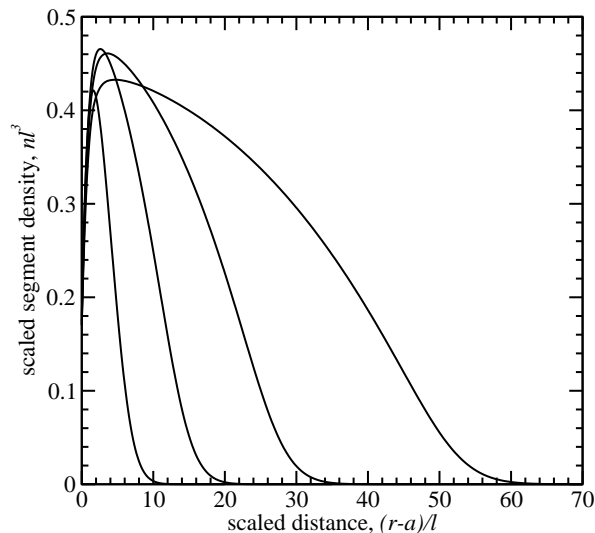


Fig. 7. The (scaled) radial segment density distribution $\phi = n(r)l^3$ of PEG chains terminally anchored to the surface of spherical (therapeutic) liposomes with radius $a = 100$ nm as a function of the (scaled) distance from the surface of the bare liposome $(r - a)/l$. The data are for representative numbers of statistical segments per chain $N = 28, 70, 140$ and 280 , with molecular weights $W \approx 2, 5, 10$ and 20 kgmol $^{-1}$. The self-consistent mean-field potential is specified according to Hill (13) with $v_2/v_1 = 3.3$, $v_2/l^3 = 0.27$, $\sigma_p l^2 = 0.072$ and $l = 0.71$ nm.

thicknesses, and electrophoretic mobilities of polystyrene latices in aqueous solution with three molecular weights of adsorbed PEO. They used the mobilities of the bare particles to infer the (varying) surface charge density as a function of ionic strength. As shown in table 4, the (apparent) charge, inferred from the standard electrokinetic model and measured mobilities of bare latices, increases with ionic strength.

With the methodology presented in section 3.4, these very inhomogeneous structures are approximated as uniform layers. Also, following Gittings and Saville, this analysis assumes that the polymer does not influence the surface charge. Table 5 summarizes the measured and inferred layer characteristics, and the electrophoretic mobilities and effective coating thicknesses are shown in figures 9 and 10.

Because adsorbed PEO produces layers with a very dense inner region and a much more permeable periphery, approximating the layers as uniform is crude. Nevertheless, varying the segment density distributions to improve the predicted mobilities is invariably met with a poorer prediction of the measured effective layer thicknesses. In particular, adopting a model with two step-like regions (a very dense and relatively thin inner layer with a much thicker and permeable outer layer) produced results very similar to those in figures 9(a)

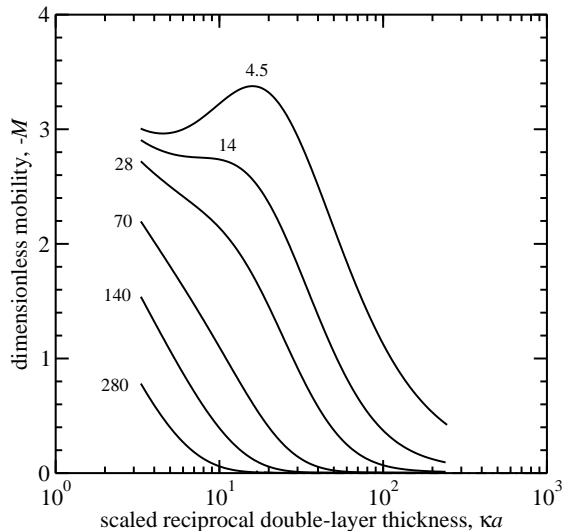


Fig. 8. The (scaled) electrophoretic mobility $M = 3\eta eV / (2\epsilon_s \epsilon_o kTE)$ of spherical liposomes with coatings of terminally anchored PEG as a function of the (scaled) reciprocal double-layer thickness κa (aqueous NaCl at $T = 25^\circ\text{C}$ with radius $a = 100$ nm) for various numbers of statistical segments per PEG chain $N = 4.5, 14, 28, 70, 140$ and 280 ; the molecular weights of the PEG chains are, respectively, $W \approx 0.35, 1, 2, 5, 10$ and 20 kgmol^{-1} . The surface charge density $\sigma_c \approx -1.95$ μCcm^{-2} at all ionic strengths. These predictions are from the full model with a self-consistent mean-field description of the PEG segment density distribution (see figure 7).

and 10(a) with a single region. This was also the case with exponentially decaying distributions. Varying the Stokes radius of the segments, while maintaining the ‘correct’ hydrodynamic layer thicknesses and adsorbed amounts, slightly improved the predicted electrophoretic mobilities, but the resulting layer thicknesses L were unrealistically large, and the resulting Stokes radius a_s was extremely small.

Comparing the model predictions in figure 9(a) with Gittings and Saville’s measurements in figure 9(b) reveals that the influence of polymer on the electrophoretic mobilities is underestimated by the model at low ionic strength, and overestimated at high ionic strength. The qualitative effects of varying the PEO molecular weight and adsorbed amount are captured relatively well, however. Comparing variations in the effective layer thicknesses of the bare and coated particles in figure 10 demonstrates that polymer attenuates the electro-viscous contribution to the drag. Even for the bare latices, variations in the effective size with ionic strength are greater than suggested by the theory. Recall, L_e reflects an increase in the apparent radius of the bare particle. Therefore, for colloids without a polymer coating, L_e equals the hydrodynamic thickness L_h only in the absence of electro-viscous drag.

Table 4

The ionic strength-charge relation for the PEO-coated polystyrene latices ($a = 78$ nm) used in the Gittings-Saville experiments (23). The surface charge densities are inferred from the measured electrophoretic mobilities of the bare latices. See table 5 for the PEO-coating parameters.

I (M)	σ_c (μCcm^{-2})
10^{-5}	0.250
10^{-4}	0.600
5×10^{-4}	0.995
10^{-3}	1.352
3.43×10^{-3}	1.713
10^{-2}	1.928

Evidently, the influence of adsorbed polymer on the surface charge depends on the ionic strength. In general, therefore, neutral polymer tends to reduce the (apparent) charge more than expected from the effect on hydrodynamic transport processes alone. Either the polymer changes the underlying charge or charge affects the polymer configuration. At very low ionic strength, a considerable portion of the diffuse double layer resides outside a uniform polymer layer, suggesting that either the polymer extends further from the interface, to increase the effective layer thickness, or the charge is diminished.

Note that polymer lowers the effective dielectric constant at the interface, thereby increasing correlations between the fixed and mobile charge, which, in turn, could decrease the degree of counterion dissociation. Note also that polarization of low-dielectric neutral polymer segments by the equilibrium electrostatic potential may increase layer thicknesses, particularly at low ionic strength when the double layer is thick and the surface potential is high. We have not explored the possibility that the Stokes radius of the segments may vary with the local polymer configuration. With large fluctuations in segment density in the periphery, the effective Stokes radius might be very small, whereas the thin dense region at the surface may produce an effective Stokes radius more representative of the segment size. The model also neglects the influence that dense polymer has on molecular diffusion and electro-migration. Therefore, while the full model improves upon earlier interpretations based on the standard model (see 23), further investigation is required.

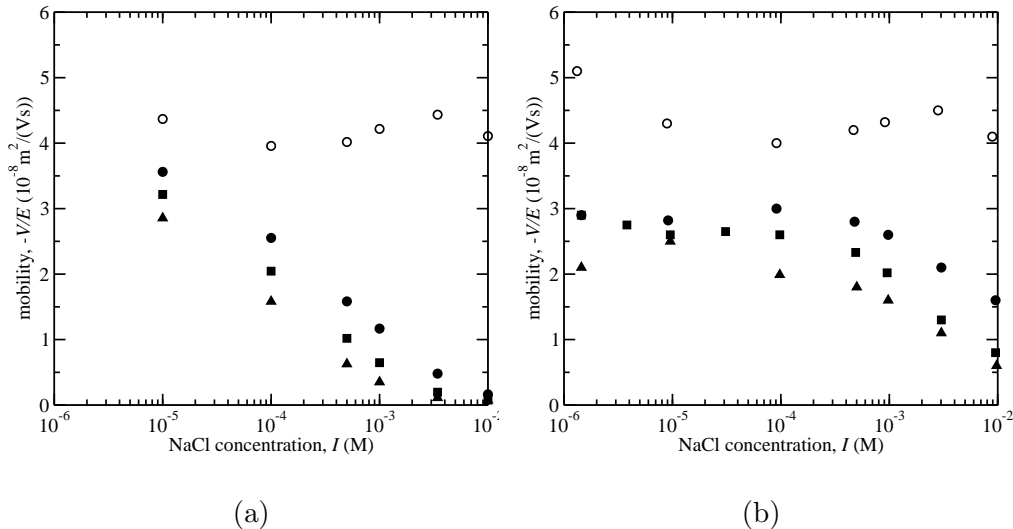


Fig. 9. Theoretical interpretation (*left*) of Gittings and Saville’s experiments (*right*) for the electrophoretic mobility V/E of polystyrene latices with coatings of adsorbed PEO as a function of the ionic strength I (aqueous NaCl at $T = 25^\circ\text{C}$) for various PEO molecular weights $W = 0$ (open circles), 23.5 (filled circles), 56 (squares) and 93.75 kgmol^{-1} (triangles). The surface charge densities and adsorbed amounts are specified according to Gittings and Saville (23) (see tables 5 and 4), and the mobilities are calculated using the full electrokinetic model with uniform layers yielding the measured hydrodynamic layer thicknesses and adsorbed amounts. The segment Stokes radius $a_s = 0.175 \text{ \AA}$ with $l = 0.71 \text{ nm}$ is from Hill’s interpretation (13) of Cohen and Khorosheva’s experiments (20) with terminally anchored PEG on multilamellar liposomes.

Table 5

Polymer layer properties for the PEO-coated polystyrene latices used in the Gittings-Saville experiments (23). The electrophoretic mobilities of the bare and ‘fuzzy’ latices are presented in figure 9. These parameters characterize the uniform layers adopted in the full electrokinetic model. See table 4 for the surface charge densities.

$W \text{ (kgmol}^{-1}\text{)}$	$\sigma_p \text{ (mgm}^{-2}\text{)}$	$L_h^1 \text{ (nm)}$	N	$L \text{ (nm)}$	$\ell \text{ (nm)}$	$L_h^2 \text{ (nm)}$
23	0.67	11.5	534	13.8	2.32	11.4
56	0.73	17.0	1270	19.8	2.76	16.9
93.75	0.59	23.5	2130	27.3	3.76	23.3

¹ From Gittings and Saville’s experiments (23).

² Calculated with uniform layers.

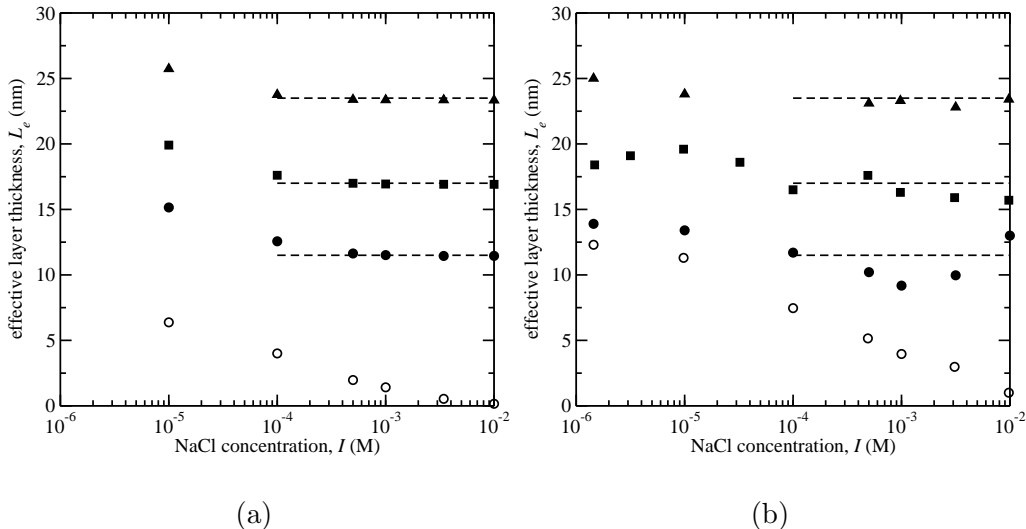


Fig. 10. Theoretical interpretation (*left*) of Gittings and Saville’s experiments (*right*) for the effective layer thickness L_e of PEO adsorbed on polystyrene latices as a function of the ionic strength I (aqueous NaCl at $T = 25^\circ\text{C}$) for various PEO molecular weights $W = 0$ (open circles), 23.5 (filled circles), 56 (squares) and 93.75 kgmol^{-1} (triangles). The surface charge densities and adsorbed amounts are specified according to Gittings and Saville (23) (see tables 5 and 4), and the effective layer thicknesses are calculated using the full electrokinetic model with uniform layers yielding the (nominal) measured hydrodynamic layer thicknesses and adsorbed amounts. The segment Stokes radius $a_s = 0.175 \text{ \AA}$ with $l = 0.71 \text{ nm}$ is from Hill’s interpretation (13) of Cohen and Khorosheva’s experiments (20) with terminally anchored PEG on multilamellar liposomes. Lines indicate the *hydrodynamic* layer thicknesses L_h .

4 The mobility of colloids with charged coatings

4.1 Thin polyelectrolyte coatings

In this section we examine moderately large particles with thin charged (polyelectrolyte) layers. The electrophoretic mobilities of colloids with radius $a = 500 \text{ nm}$ in figure 11 show the effect of varying the (uniform) polyelectrolyte density while maintaining a constant layer thickness $L = 0.25\sqrt{10^3} \text{ nm}$. As the ionic strength increases from $I = 10^{-6}$ to 10 M , κa spans the range 1.64–5200; the double-layer thickness is comparable to the coating thickness when $I \approx 1.5 \text{ mM}$. The densities of the coatings span the range $n_0 \approx 0.13\text{--}1.1 \text{ M}$, so with a segment Stokes radius $a_s = 0.95 \text{ \AA}$ the respective Brinkman screening lengths span the range $\ell \approx 2.6\text{--}0.89 \text{ nm}$. Note that Stokes radius of the (monomer) segments adopted here is an approximate value for poly(styrene

sulfonate) monomer segments inferred by Hill (13) from experiments by Cottet et al. (24) reporting the electrophoretic mobilities and hydrodynamic radii of associating copolymer micelles (13) (see § 4.3).

The fixed charge density is assumed proportional to the segment (monomer) density and, furthermore, is specified assuming one elementary charge per Bjerrum length l_B of the polyelectrolyte contour length. Accordingly, the charge density $n_0^f = (2.5/7.1)n_0$; each segment has length $l = 2.5 \text{ \AA}$ with $l_B = e^2/(4\pi\epsilon_o\epsilon_s kT) \approx 7.1 \text{ \AA}$. This simple model accounts for *counterion condensation*, which, according to Manning’s well-known theory (25), limits the *effective* linear charge density to el_B^{-1} when the *actual* linear charge density exceeds this value. For highly charged polyelectrolytes, *e.g.*, poly(styrene sulfonate) with degree of sulfonation greater than 40 percent, accounting for counterion condensation in this way leads to ‘reasonable’ electrostatic potentials (Donnan potentials) inside the layer. When interpreting measured electrophoretic mobilities, the methodology infers a Stokes radius for the monomer segments $a_s \approx 0.95 \text{ \AA}$, which, in contrast to PEG brushes (see § 3.4 and § 3.5), is representative of the segment (monomer) length, $l_m \approx 2.5 \text{ \AA}$.

The moderately large particle radius ($a = 500 \text{ nm}$) facilitates a comparison of the full model with analytical solutions valid as $\kappa a \rightarrow \infty$ with $\kappa L \gg 1$. Levine et al.’s theory (5, Eqn. (21)) (*dashed* lines) is in excellent agreement with the numerically exact results when the ionic strength is high, *i.e.*, when $\kappa L \gg 1$ and the Debye-Hückel approximation is justified ($\psi < 2kT/e$). The range of ionic strengths over which their formula is accurate increases with decreasing charge density, suggesting that the Debye-Hückel approximation is more restrictive here than the condition $\kappa L \gg 1$. Ohshima’s theory (19, Eqn. (11.4.18)) (*dash-dotted* lines), which neglects the viscous stress at the grafting surface, is restricted here to dense layers with $L/\ell > 8$.

At high ionic strength, viscous drag at the grafting surface leads to lower mobilities than predicted by Ohshima’s theory. This is demonstrated most clearly by the particle with the least dense layer⁴ (case 1 in figure 11). Under free-draining conditions—the regime that underlies the high-ionic-strength-limit of Ohshima’s theory—the electrophoretic mobility of this particle is expected to be the highest, since the drag coefficient of the segments is least because of the small, but finite, (hydrodynamic) volume fraction $\phi_s = n(4/3)\pi a_s^3 \sim 10^{-4}$. However, because the layer is sufficiently permeable *and* thin, viscous stress from the substrate also contributes to the drag. Consequently, this particle has the lowest mobility at high ionic strength. At lower (intermediate) ionic strength, an increasing fraction of the mobile charge resides beyond the coat-

⁴ Close examination of figure 11 reveals that Ohshima’s theory (*dash-dotted* lines) yields a mobility about 10 percent higher (in magnitude) than the full theory at high ionic strength.

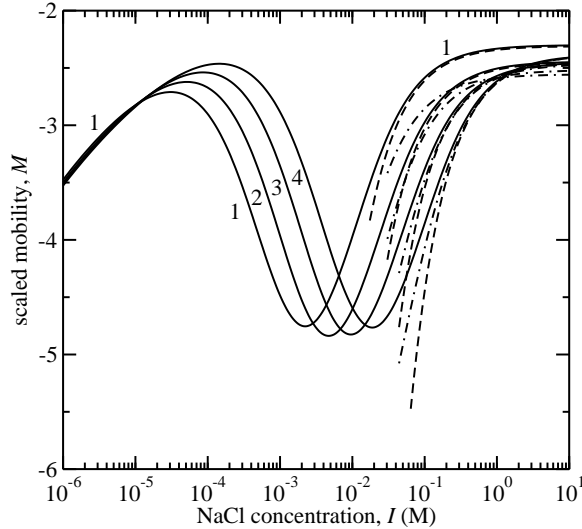


Fig. 11. The (scaled) electrophoretic mobility $M = 3\eta eV / (2\epsilon_s \epsilon_o kTE)$ of spherical colloids with relatively thin, uniform coatings of charged polymer as a function of the ionic strength I (aqueous NaCl at $T = 25^\circ\text{C}$): $a = 500$ nm; $L = 0.25\sqrt{10^3}$ nm; $a_s = 0.95$ Å; $n_0 \approx 0.132, 0.263, 0.526$ and 1.05 M (labeled 1–4 with $\ell \approx 2.6, 1.8, 1.3$ and 0.89 nm); and $n_0^f = (2.5/7.1)n_0$. *Solid* lines are the full model with uniform (step-like) segment density distributions, *dash-dotted* lines are Ohshima's theory for thin uniform layers with $L/\ell \gg 1$ (19, Eqn. (11.4.18)), and *dashed* lines are Levine et al.'s theory for thin uniform layers with arbitrary L/ℓ and $|\psi| < 2kT/e$ (5, Eqn. (21)).

ing, and the mobility might therefore be expected to increase with the total charge (increasing segment density). However, the particles with the highest charge are more susceptible to polarization, and this leads to an inverse relationship between the charge and mobility. Nevertheless, at even lower ionic strength, particles with higher charge eventually exhibit higher mobilities. In this limit, the total charge, rather than the slightly larger hydrodynamic radius (friction coefficient), has the greater influence on the mobility.

4.2 Glycocalyx on human erythrocytes

Levine et al. (5) developed their theory to interpret the electrophoretic mobility of human erythrocytes, revealing that the glycocalyx charge density is sufficiently high to produce an electrostatic potential that violates the Debye-Hückel approximation. Sharp and Brooks (6) then solved the planar electrokinetic transport problem numerically, relaxing the Debye-Hückel approximation, and they were able to infer a layer thickness of $L = 7.8$ Å, with segment and charge densities of $n_0 \approx 0.0690$ and $n_0^f \approx 0.0472$ M, respectively, at ionic

strengths in the range $I = 10\text{--}160$ mM. Note that, with a segment Stokes radius $a_s = 7$ Å and drag coefficient $F_s = 1$, the Brinkman screening length is $\ell \approx 1.35$ nm. Sharp and Brooks' calculations are limited by the finite particle size (polarization and relaxation), so it remains to establish the range of ionic strengths over which the flat-plate approximation is accurate. We will also briefly examine the effect of varying the layer thickness, while maintaining a constant mass and charge.

The mobility-ionic strength relationship in figure 12 verifies the accuracy of Ohshima's theory (*dash-dotted* lines) for this problem when the ionic strength is greater than approximately 5 mM. Clearly, Levine et al.'s theory (*dashed* lines) is limited here by the Debye-Hückel approximation, even at low ionic strength. At high ionic strength, however, a close examination reveals that their expression is more accurate than Ohshima's, because it accounts for viscous stress on the bare surface. Finally, the 'exact' results (*solid* lines) show that the particle size ($a = 3.5$ μm) influences the mobility when the ionic strength is less than about 10 mM, *i.e.*, when $\kappa a < 10^3$.

To assess the effect of expansion and contraction of the layers due to electrostatic stiffening of the polyelectrolyte at low ionic strength, we perturbed Sharp and Brooks' data (case 2) by halving (case 1) and doubling (case 3) the (glycocaylx) layer thickness. Because the particle radius is large ($a = 3.5$ μm), the changes are accompanied by respective doubling and halving of the segment and charge densities. Expansion decreases the segment density, thereby decreasing the fixed charge density and increasing the layer permeability. To account for the influence of density on the segment drag coefficient, the Stokes radius of the segments is $a_s = 3.5$ Å, which yields a slightly larger Brinkman screening length ($\ell = 1.73$ Å) than that of Sharp and Brooks when $L = 7.8$ Å. The hydrodynamic volume fraction inferred by Sharp and Brooks' parameters suggests that varying the density should also affect the segment drag coefficient. Indeed, we have interpreted their Stokes radius as the product $a_s F_s(\phi_s)$, so changing the density also changes the drag coefficient according to the change in (hydrodynamic) volume fraction. The sensitivity of the mobility to the layer thickness and, hence, density, is most pronounced at an ionic strength of approximately 1 mM. Because polarization and relaxation are significant under these conditions, numerically exact solutions could benefit future studies, even with relatively large particles.

4.3 Poly(styrene sulfonate) micelles

Finally we turn to 'small' colloids with relatively thick charged (sodium poly(styrene sulfonate)) layers. Figure 13 shows the mobilities of two representative hydrophobically associating copolymer micelles over a range of ionic strengths.

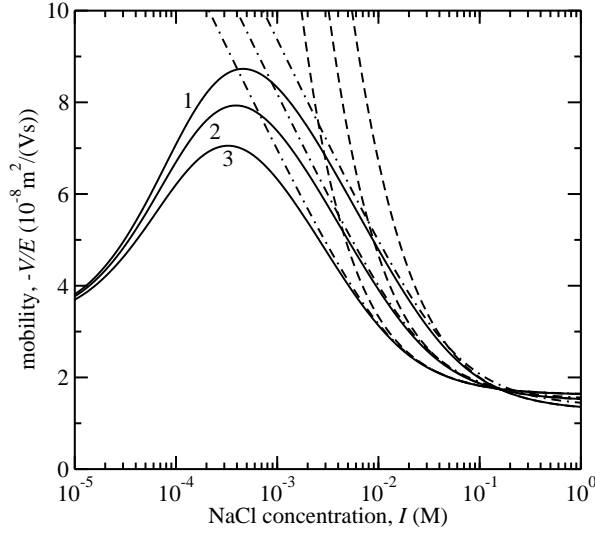


Fig. 12. The electrophoretic mobility V/E of human erythrocytes as a function of the ionic strength I (aqueous NaCl at $T = 25^\circ\text{C}$): $a = 3.5 \mu\text{m}$; $L = 7.8/2, 7.8$ and $7.8 \times 2 \text{ nm}$ (labeled 1–3, respectively); $a_s = 3.5 \text{ \AA}$; $n_0 \approx 0.0690 \times 2, 0.0690$ and $0.0690/2 \text{ M}$ (labeled 1–3 with $\ell \approx 2.52, 1.73$ and 1.16 nm , respectively); and $n_0^f = (0.0472/0.0690)n_0$. *Solid* lines are the full model with uniform (step-like) segment density distributions, *dash-dotted* lines are Ohshima’s theory for thin uniform layers with $L/\ell \gg 1$ (19, Eqn. (11.4.18)), and *dashed* lines are Levine et al.’s theory for thin uniform layers with arbitrary L/ℓ and $|\psi| < 2kT/e$ (5, Eqn. (21)).

The radii of the hydrophobic cores, a , and of the respective particles as a whole, $L_h + a$, are based on neutron diffusion and light scattering measurements, respectively (24). Furthermore, the charged coronas are assumed uniform, with *monomer* densities

$$n_0 = \frac{n_a N_m}{(4/3)\pi a^3 [(1 + L/a)^3 - 1]}, \quad (61)$$

where n_a is the aggregation number and N_m is the number of poly(styrene sulfonate) monomers per chain. Note that L and L_h are specified according to Eqn. (60); these and other characteristics are listed in table 6.

The micelles assembled from the longest polyelectrolyte chains (case 2) have a much larger hydrodynamic radius $L_h + a \approx 80 \text{ nm}$. The smaller aggregation number $n_a \approx 35$ manifests in a relatively low segment density $n_0 \approx 0.0074 \text{ M}$, and, hence, lower density of charged sites $n_0^f \approx (2.5/7.1)n_0 \approx 0.0026 \text{ M}$. Note that, following the discussion in section 4.1, allowing for counterion condensation yields an effective valence for *monomer* segments $z \approx -2.5/7.1$. The total charge, which is proportional to $zN_m n_a$, is only 30 percent lower, however. Clearly, the lower segment density results in a much more permeable particle, as evidenced by the large Brinkman screening length $\ell \approx 11.2 \text{ nm}$.

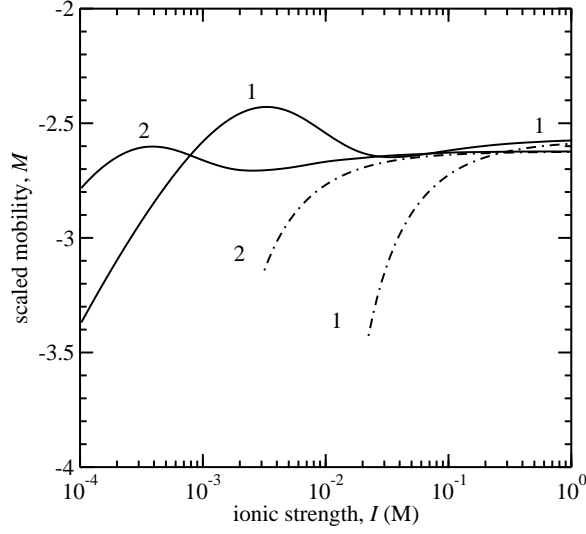


Fig. 13. The (scaled) electrophoretic mobility $M = 3\eta eV / (2\epsilon_s \epsilon_o kTE)$ of spherical colloids with relatively thick, uniform coatings of charged polymer as a function of the ionic strength I (aqueous NaCl at $T = 25^\circ\text{C}$). See table 6 for parameters. For both particles, $a_s = 0.95 \text{ \AA}$ and $n_0^f = (2.5/7.1)n_0$. *Solid* lines are the full model with uniform (step-like) segment density distributions, and *dash-dotted* lines are Ohshima's theory for spherical polyelectrolytes (19, Eqn. (11.3.11)).

Table 6

Parameters derived from data (24) characterizing two micelles (with charged coronas) whose electrophoretic mobilities are shown in figure 13: $a_s = 0.95 \text{ \AA}$ and $n_0^f = (2.5/7.1)n_0$.

case	a (nm)	N	n_a	$Nn_a 10^{-3}$	$L_h + a$ ¹ (nm)
1	5.2	227	85	19.3	42
2	2.6	404	35	14.1	80

case	$L + a$ ² (nm)	n_0 (M)	n_0^f (M)	ℓ (nm)	L/ℓ	L/a
1	45.4	0.082	0.029	3.31	12	7.7
2	91.2	0.0074	0.0026	11.2	7.9	34

¹ Actual (measured) hydrodynamic size.

² From the measured hydrodynamic size and Eqn. (60).

Following the methodology underlying Eqn. (60), the actual 'coating' thickness $L \approx 89 \text{ nm}$ is about 12 percent smaller than the chain contour length $l_c \approx 404 \times 0.25 = 101 \text{ nm}$, indicating that the chains are strongly stretched.

Note that the permeabilities in table 6 have been established from electrophoretic mobilities reported by Cottet et al. (24) (at a single ionic strength yielding

$\kappa^{-1} \approx 2 \text{ nm}$): $V/E \approx -3.4 \times 10^{-8}$ (case 1) and $-3.7 \times 10^{-8} \text{ m}^2/(\text{Vs})$ (case 2). From the high-ionic-strength limit of the full electrokinetic model

$$V/E = ze/(6\pi\eta a_s F_s), \quad (62)$$

where z is the effective valence of a segment, these mobilities and the ‘coating’ parameters in table 6 suggest a Stokes radius for *monomer* segments $a_s \approx 0.95 \text{ \AA}$ (13).

Equation (62) is the free-draining limit of Ohshima’s (19, Eqn. (11.3.11)) and Hermans and Fujita’s theories for uniformly charged spherical polyelectrolytes (19). Solutions of the full electrokinetic model show that Eqn. (62) also applies to non-uniform layers when the segment and charge densities are proportional to each other, and the coatings are thick enough for the viscous stress on the substrate to be small compared to the frictional drag on the polymer (12).

Figure 13 shows that the mobilities predicted by the full model do not vary significantly over a wide range of electrolyte concentrations. While Ohshima’s theory (*dash-dotted* lines) is in good agreement with the ‘exact’ results at very high ionic strength, the correction it provides to Eqn. (62) is very small. The analytical theory compares more favorably with the ‘exact’ results for the larger particle, *i.e.*, case 1 with larger $\kappa(a + L)$, despite the smaller value of L/ℓ . Again, this points to the significance of polarization and relaxation. Note that the high ionic strength at which Eqn. (62) applies usually permits polarization and relaxation to be neglected. For these relatively small and highly charged particles, however, the analytical theory is accurate only at inordinately high ionic strength.

In contrast to bare particles and, indeed, particles with neutral coatings, the mobilities reach minimum values at intermediate ionic strengths. Here, the minima coincide with the electrostatic potential inside the polyelectrolyte passing through $|\psi| \approx 2kT/e$. Note that the potentials would be significantly higher if we had not accounted for counterion condensation, at least in the manner described in section 4.1. With a characteristic particle radius $a + L_h$, $\kappa(L_h + a) \approx 14$ (case 1) and 26 (case 2) when $I = 10 \text{ mM}$, for example. Moreover, when $I = 1 \text{ M}$, $\kappa(L_h + a) \approx 140$ (case 1) and 260 (case 2). Once again, with the mobilities shown in figure 13, we see that polarization and relaxation is important when the double-layer thickness is greater than a few percent of the characteristic particle size.

At low ionic strength, the mobility reflects a balance between the electrical force on the fixed charge, which is proportional to zNn_a , and the hydrodynamic drag, which is proportional to $a + L_h \sim N^\nu$ ($0 < \nu < 1$). It follows that the mobility should increase with the aggregation number, which is indeed the case at low ionic strength. Because the mobility is also susceptible to

polarization, and not all the counter charge resides beyond the polymer, the permeability and particle size also play a role.

As expected, calculations (not reported here) with twice the segment Stokes radius ($a_s = 1.9 \text{ \AA}$) yield mobilities (at high ionic strength) that are half those in figure 13. At low ionic strength, the mobilities are attenuated only slightly, whereas at intermediate ionic strengths the minima cease to exist and the mobility (magnitude) increases monotonically with decreasing ionic strength. Evidently, decreasing the permeability decreases the effectiveness of convection in polarizing the double layer, as expected from the inferences drawn in section 3.3 for neutral layers.

Note that the thickness and density of terminally anchored polyelectrolytes *can* vary significantly with the bulk ionic strength. Such variations have been neglected entirely. At low ionic strength, the effective Kuhn length increases because of weakly screened electrostatic repulsion among charged monomers along the backbone (a so-called short-range interaction). This can lead to layers whose hydrodynamic thickness is comparable to the polymer contour length. Here, however, the relatively high ionic strength at which the mobilities and sizes were reported suggests that excluded volume (long-range) interactions are dominant because of the high grafting density. At lower densities, electrostatic interactions can be much more influential (see 26). Moreover, grafted chains may ‘collapse’ at high ionic strength if the grafting density is low, yielding much thinner, dense layers. The varying segment and charge density that accompany such structural changes also affect the electrostatic potential, which, in turn, influences the ionic strength at which polarization affects the mobility. A quantitative interpretation of these processes would benefit greatly from experiments reporting mobilities and hydrodynamic radii over a range of ionic strengths.

5 Summary

The ‘full’ electrokinetic model of Hill, Saville and Russel (12) was applied to a variety of ‘soft’ colloids. Analogously to O’Brien and White’s solutions of the standard electrokinetic model, the methodology removes all approximations imposed by earlier theories. Because of polarization and relaxation, exact solutions of the full model were demonstrated to be as important for ‘soft’ colloids as the O’Brien and White methodology is for ‘bare’ particles.

A simple approach was described to link characteristics, such as the polymer adsorbed amount and molecular weight, to key parameters in the model, namely the polymer layer density, permeability and thickness, and their radial distributions. Calculations revealed that the *hydrodynamic* layer thickness, as

distinguished from the actual thickness, is the single most important layer characteristic influencing the mobility. A convenient (and often reasonable) approximation is to set the hydrodynamic thickness of a uniform layer to its actual thickness minus the Brinkman screening length. It is then straightforward (*e.g.*, Eqn. 60) to relate the actual thickness, density and permeability (via the Stokes radius of the segments) of a uniform coating to the grafting density (or adsorbed amount) and polymer molecular weight for a non-uniform layer.

The full model was compared to Ohshima's analytical theories for thin uniform, neutral layers. As expected, good agreement was found when the double layer and coating are very thin compared to the particle radius (less than a few percent) and polarization and relaxation are negligible. Figures 4 and 5 provide a useful reference for assessing the (coupled) influences of layer thickness, double-layer thickness and particle size on polarization and relaxation. Contrary to expectations, flat-plate approximations breakdown at very high ionic strength. However, because the mobility under these conditions is small, this unexpected behavior is revealed only on logarithmically scaled mobility axes. Neutral polymer was identified as attenuating polarization, but polarization and relaxation still influence the mobility of particles with radii less than a few microns.

The full model was applied to interpret the mobilities of (stealth) liposomes with terminally anchored poly(ethylene glycol) (PEG). Approximating the layers as uniform, with the 'correct' hydrodynamic layer thickness, provided a close correspondence with experiments (20) *and* calculations that invoke much more involved computations of the polymer-layer structure (13). There remain relatively small differences between theory and experiment when the ionic strength and polymer grafting density are low (13). Polymer anchored to the surface of fluid-like membranes poses complications beyond the scope of the current electrokinetic model, which assumes immobile surface charge and polymer. Nevertheless, based on earlier attempts to establish the Stokes radius of aqueous PEG statistical segments, theoretical predictions of the mobilities of 100 nm radius (therapeutic) stealth liposomes were presented with a typical grafting density and a variety of polymer molecular weights. These calculations clearly demonstrate the extent to which neutral polymer coatings decrease the apparent ζ -potential, even though the actual charge remains constant.

When applied to interpret the mobilities *and* hydrodynamic sizes of polystyrene latices stabilized in aqueous electrolyte by adsorbed poly(ethylene oxide) (PEO) homopolymer, the theory captured only the qualitative aspects of the available data (23). Moreover, measured mobilities at low ionic strength are lower than suggested by the theory. Evidently, adsorption of neutral polymer lowers the charge, or the electric field due to charge alters the polymer conformation. While model parameters (for the polymer layers) can be adjusted to provide a

good fit to measured electrophoretic mobilities, this is inevitably accompanied by a poorer prediction of the (measured) hydrodynamic layer thickness.

For particles with charged layers, the full model corroborated approximate theories in their respective domains of applicability (*e.g.*, thin layers, at high ionic strength, with low electrostatic potentials). For example, we adopted parameters that characterize human erythrocytes, as established from theoretical and experimental studies by Brooks and coworkers. We also compared the full model with approximate analytical solutions for particles with ‘thick’ charged layers. These parameters were based on measured dimensions (at one ionic strength) of polyelectrolyte micelles (with poly(styrene sulfonate) coronas). Extrapolating the electrophoretic mobilities to higher and lower ionic strength (with fixed dimensions and charge) revealed that analytical theory (after Ohshima and Hermans and Fujita) is accurate (for these particles) only at inordinately high ionic strength. This shortcoming reflects the small size of the micelles, their high charge density, and, hence, the strong influence of polarization and relaxation. Note that the calculations invoked counterion condensation, which places an upper limit on the effective charge and, therefore, limits the prevailing electrostatic potential.

At present, the availability of sufficiently well-characterized electrokinetic data for soft spheres is limited, so we trust that the model and its availability will stimulate further experimental studies. Again, it should be noted that, while this paper focused on the electrophoretic mobility, the electrokinetic model also provides characteristics (*e.g.*, complex polarizability/conductivity (27; 28) and dynamic mobility) derived from a variety of electrokinetic experiments.

RJH acknowledges support from the Natural Sciences and Engineering Research Council of Canada (NSERC), through grant number 204542, and the Canada Research Chairs program (Tier II).

References

- [1] J. L. Anderson, Y. Solomentsev, Hydrodynamic effects of surface layers on colloidal particles, *Chem. Eng. Comm.* 148–150 (1996) 291–314.
- [2] S. S. Dukhin, N. M. Semnikhin, Theory of double layer polarization and its effect on the electrokinetic and electrooptical phenomena and the dielectric permeability of dispersed systems, *Kolloidn. Zh.* 32 (1970) 360.
- [3] L. A. Rosen, J. C. Baygents, D. A. Saville, The interpretation of dielectric response measurements on colloidal dispersions using the dynamic stern layer model, *J. Chem. Phys.* 98 (5) (1993) 4183–4194.
- [4] R. W. O’Brien, L. R. White, Electrophoretic mobility of a spherical colloidal particle, *J. Chem. Soc., Faraday Trans. II* 74 (1978) 1607–1626.

- [5] S. Levine, K. Levine, K. A. Sharp, D. E. Brooks, Theory of the electrokinetic behavior of human erythrocytes, *Biophys. J.* 42 (1983) 127–135.
- [6] K. A. Sharp, D. E. Brooks, Calculation of the electrophoretic mobility of a particle bearing bound polyelectrolyte using the nonlinear Poisson-Boltzmann equation, *Biophys. J.* 47 (1985) 563–566.
- [7] J. J. Hermans, H. Fujita, Electrophoresis of charged polymer molecules with partial free drainage, *Koninkl. Ned. Akad. Wetenschap. Proc.* B58 (1955) 182.
- [8] J. J. Hermans, Sedimentation and electrophoresis of porous spheres, *J. Polym. Sci.* 18 (1955) 527–534.
- [9] H. Ohshima, Approximate analytical expressions for the electrophoretic mobility of colloidal particles with surface-charge layers, *J. Colloid Interface Sci.* 130 (1989) 281–282.
- [10] C. C. Ho, T. Kondo, N. Muramatsu, H. Ohshima, Surface structure of natural rubber latex particles from electrophoretic mobility, *J. Colloid Interface Sci.* 178 (1996) 442–445.
- [11] D. A. Saville, Electrokinetic properties of fuzzy colloidal particles, *J. Colloid Interface Sci.* 222 (2000) 137–145.
- [12] R. J. Hill, D. A. Saville, W. B. Russel, Electrophoresis of spherical polymer-coated colloidal particles, *J. Colloid Interface Sci.* 258 (2003) 56–74.
- [13] R. J. Hill, Hydrodynamics and electrokinetics of spherical liposomes with coatings of terminally anchored poly(ethylene glycol): Numerically exact electrokinetics with self-consistent mean-field polymer, *Phys. Rev. E* 70 (2004) 051046.
- [14] D. L. Koch, A. S. Sangani, Particle pressure and marginal stability limits for a homogeneous monodisperse gas fluidized bed: Kinetic theory and numerical simulations, *J. Fluid Mech.* 400 (1999) 229–263.
- [15] S. Kim, W. B. Russel, Modelling of porous media by renormalization of the Stokes equations, *J. Fluid Mech.* 154 (1985) 269–286.
- [16] I. D. Howells, Drag on fixed beds of fibres in slow flow, *J. Fluid Mech.* 355 (1998) 163–192.
- [17] G. W. Jackson, D. F. James, The permeability of fibrous porous-media, *Can. J. Chem. Eng.* 64 (3) (1986) 364–374.
- [18] P. M. Biesheuval, Ionizable polyelectrolyte brushes: brush height and electrostatic interaction, *J. Colloid Interface Sci.* 275 (1) (2004) 97–106.
- [19] H. Ohshima, Electrophoresis of soft particles, *Advances in Colloid and Interface Science* 62 (1995) 189–235.
- [20] J. A. Cohen, V. A. Khorosheva, Electrokinetic measurement of hydrodynamic properties of grafted polymer layers on liposome surfaces, *Colloids and Surfaces A: Physicochemical and Engineering Aspects* 195 (2001) 113–127.
- [21] G. J. Fleer, M. A. Cohen Stuart, J. M. H. M. Scheutjens, T. Cosgrove, B. Vincent, *Polymers at Interfaces*, Chapman and Hall, 1988.
- [22] G. J. Fleer, J. van Male, Analytical approximations to the Scheutjens-Fleer

- theory for polymer adsorption from dilute solution. 2. Adsorbed amounts and structure of the adsorbed layer, *Macromolecules* 32 (3) (1999) 845–862.
- [23] M. R. Gittings, D. A. Saville, The electrokinetic behavior of bare and polymer-coated latices, *Langmuir* 16 (2000) 6416–6421.
- [24] P. Cottet, H. Gareil, P. Guenoun, F. Muller, M. Delsanti, P. Lixon, J. W. Mays, J. Yang, Capillary electrophoresis of associative diblock copolymers, *J. Chromatography A* 939 (2001) 109–121.
- [25] G. S. Manning, Limiting laws and counterion condensation in polyelectrolyte solutions i. colligative properties, *J. Chem. Phys.* 51 (3) (1969) 924–933.
- [26] R. Hariharan, C. Biver, J. Mays, W. B. Russel, Ionic strength and curvature effects in flat and highly curved polyelectrolyte brushes, *Macromolecules* 31 (1998) 7506–7513.
- [27] R. J. Hill, D. A. Saville, W. B. Russel, Polarizability and complex conductivity of dilute suspensions of spherical colloidal particles with uncharged (neutral) polymer coatings, *J. Colloid Interface Sci.* 268 (2003) 230–245.
- [28] R. J. Hill, D. A. Saville, W. B. Russel, Polarizability and complex conductivity of dilute suspensions of spherical colloidal particles with charged (polyelectrolyte) coatings, *J. Colloid Interface Sci.* 263 (2) (2003) 478–497.